NANO LETTERS

Letter

pubs.acs.org/NanoLett

Revealing the Interfacial Self-Assembly Pathway of Large-Scale, Highly-Ordered, Nanoparticle/Polymer Monolayer Arrays at an Air/Water Interface

Shisheng Xiong,[†,⊥] Darren R. Dunphy,*[,†] Dan C. Wilkinson,[†] Zhang Jiang,[‡] Joseph Strzalka,[‡] Jin Wang,[‡] Yongrui Su,[§] Juan J. de Pablo,[§] and C. Jeffrey Brinker*[,†,∥]

[†]Department of Chemical and Nuclear Engineering, University of New Mexico/NSF Center for Micro-Engineered Materials, Albuquerque, New Mexico 87131, United States

[‡]Advanced Photon Source, Argonne National Laboratory, Argonne, Illinois 60439, United States

[§]Institute for Molecular Engineering, University of Chicago, Chicago Illinois 60637, United States

[∥]Advanced Materials Laboratory, Sandia National Laboratories, Albuquerque, New Mexico 87106, United States

Supporting Information

ABSTRACT: The pathway of interfacial self-assembly of large-scale, highly ordered 2D nanoparticle/polymer monolayer or bilayer arrays from a toluene solution at an air/water interface was investigated using grazing-incidence small-angle scattering at a synchrotron source. Interfacial-assembly of the ordered nanoparticle/polymer array was found to occur through two stages: formation of an incipient randomly close-packed interfacial monolayer followed by compression of the monolayer to form a close-packed lattice driven by solvent evaporation from the polymer. Because the nanoparticles are hydrophobic, they localize exclusively to the polymer−air interface during self-assembly, creating a through thickness asymmetric film as confirmed by X-ray reflectivity. The interfacial self-assembly approach can be extended to form binary NP/polymer arrays. It is anticipated that by understanding the interfacial self-assembly pathway, this simple evaporative procedure could be conducted as a continuous process amenable to large area nanoparticle-based manufacturing needed for emerging energy technologies.

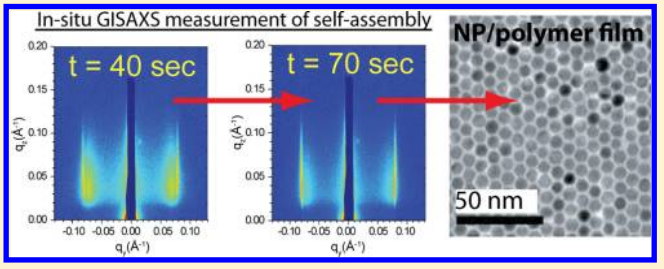

KEYWORDS: *Interfacial assembly, GISAXS, nanoparticle, polymer, nanocomposite, monolayer array*

Assembly of synthetic nanoparticles (NPs) or NPs derived from biology (e.g., viruses)[1] into two-dimensional arrays enables the positioning of functional building blocks into a well-defined close-packed planar volume, facilitating integration of NP lattices into photonic[2,3] and electronic architectures[4] as well as forming a unique structured interface for investigations of 2D phenomena such as energy transfer[5] or catalysis.[6] Importantly, the functional properties of these NP materials are expected to be highly sensitive to structural factors such as coordination number, degree of long-range order, or defect density, requiring the development of robust self-assembly pathways applicable to the deposition of NP lattices onto arbitrary substrates over macroscopic length scales. To this end, 2D NP assembly has been demonstrated using several methods, including electrostatic adsorption,[7] Langmuir−Blodgett deposition,[8,9] assembly at the air/liquid interface during solvent evaporation or on a water surface,[10−13] and convective assembly from a receding meniscus.[1] Recently, we have introduced a new rapid and facile interfacial assembly route to synthesize ordered 2D nanoparticle/polymer monolayers, wherein a droplet of a solution of hydrophobic alkane thiol derivatized NPs and hydrophobic polymers dissolved in a volatile solvent not miscible in water (e.g., toluene or chloroform) is dispensed onto a water surface (Figure 1A).[2,14,15] Rapid droplet spreading and phase separation of NPs to the polymer/air interface (vide infra) followed by contact line pinning and solvent evaporation from a receding parabolically shaped drying line drives self-assembly of a closed packed 2D NP monolayer localized at the polymer/air interface, which is supported by a thin (10−100 nm thick) polymer film. This rapid (<1 to several seconds depending on the evaporation rate) method produces highly ordered NP lattices (Figure 1B, with a larger area image given in Figure S1 in Supporting Information) over large areas (>100 cm^2) that are amenable to conformal transfer to any substrate and have the ability to span across open gaps such as those found in photonic architectures.[2,3] Preliminary results show that interfacial assembly is also a viable route to rapidly form binary NP lattices (Figure 1B, inset, with a larger area image presented as Supporting Information Figure S2).[11,12]

Received: November 17, 2012
Revised: January 24, 2013
Published: January 29, 2013

ACS Publications © 2013 American Chemical Society

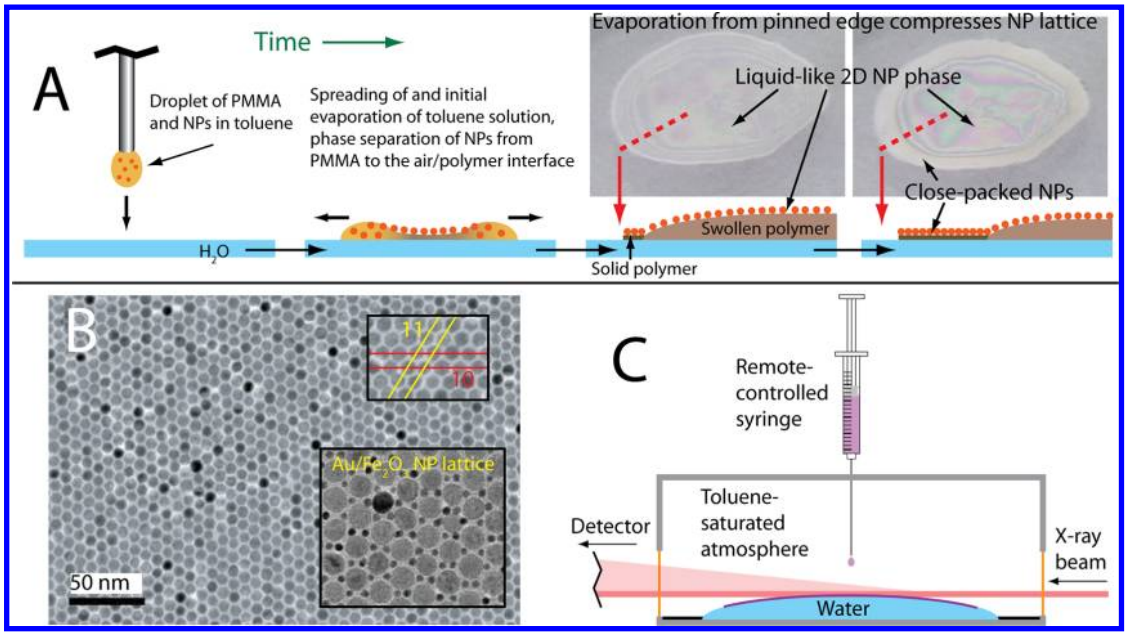

Figure 1. (A) Postulated self-assembly mechanism for formation of NP/polymer films. Images are of a Au NP/PMMA film during self-assembly, showing the recession of a parabolic shaped (in cross section) drying line after an initial rapid spreading following droplet application to the water surface (a movie of the complete film formation process, from which these images are taken, is attached as Supporting Information). (B) Plan-view TEM image of a Au NP/PMMA film showing the extended close-packed 2D NP array. Upper inset: lattice planes of the NP array. Lower inset: Binary Au/Fe_2O_3/PMMA film (nominal NP diameter = 5.5 nm for Au and 15 nm for Fe_2O_3, mole ratio = 2:1 Au/Fe_2O_3). (C) Experimental configuration used to study the self-assembly of Au NP/PMMA films in real time using GISAXS.

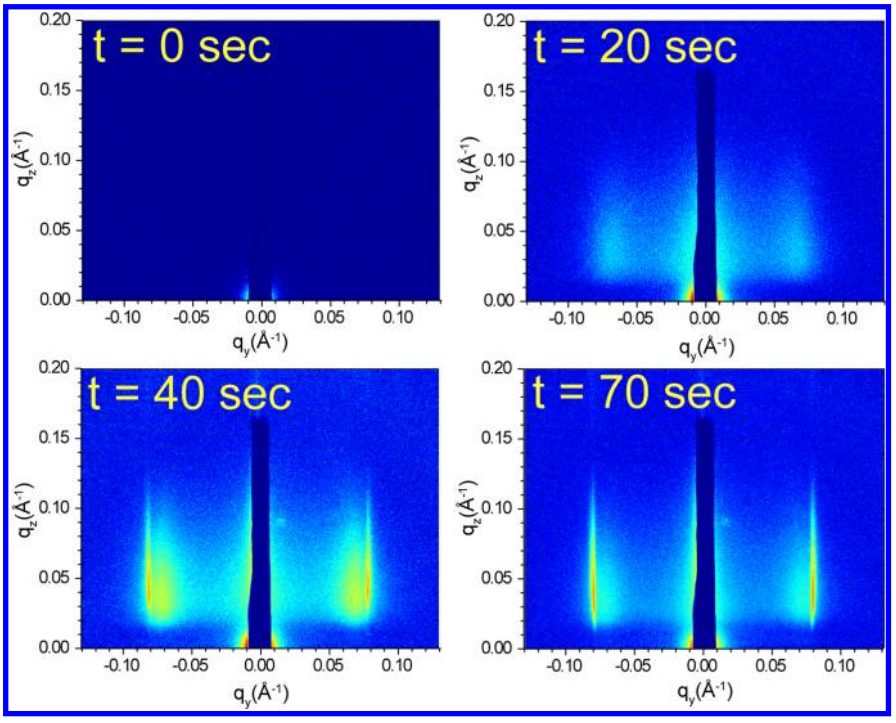

Figure 2. Sample 2D detector images obtained during the self-assembly of a Au NP/PMMA film (mass ratio 2:1), showing the initial appearance at t = 20 s of a diffuse feature indicative of a nonclose packed NP monolayer film at q_y = ca. 0.07 Å followed by the transformation of this phase to a well-ordered 2D NP lattice during film drying (q_y = ~0.08 for this second lattice). In these images, intensity is scaled logarithmically.

As for other methods of NP array formation, a fundamental understanding of the interfacial self-assembly pathway is needed to optimize film quality,[10,13] control structural parameters such as position of NPs relative to the polymer layer, and generate routes to nonhexagonally packed and binary 2D NP arrays.[12] This understanding is also essential for transforming NP assembly from a slow batch process to a rapid continuous process amenable to large area manufacturing. Here, we investigate the mechanism of interfacial assembly of polymer/NP arrays using in situ grazing incidence small-angle X-ray scattering (GISAXS) performed at a synchrotron source.[1,16−20] In GISAXS, an X-ray beam is incident upon a supported film at

dx.doi.org/10.1021/nl304253y | Nano Lett. 2013, 13, 1041−1046

an angle greater than the critical angle of the film but less than that of the support, maximizing the interaction of the beam with the film nanostructure and enabling the investigation of rapid self-assembly processes in films as thin as one monolayer under ambient conditions. In situ GISAXS studies were performed at the Argonne National Laboratories Advanced Photon Source on beamline 8ID,[19] using an X-ray wavelength of 1.675 Å, a beam size of 100 × 200 μm, and a sample to detector (Marr 2048 × 2048 CCD) distance of 1307 mm. Conditions for the self-assembly of NP/polymer films were based on previously reported procedures.[2,14,15] Dodecane-thiol protected Au NPs (core diameter 5.5 nm as determined by TEM, synthesized using a procedure modified from the literature;[21] see Supporting Information for full details) were dissolved in toluene containing 5−10 mg/mL poly(methyl methacrylate) (PMMA, M_w = 996 000). The experimental setup used for our studies is diagramed in Figure 1C. A ca. 75 × 75 mm reservoir of water (2 mL) was entrapped on a Si substrate by a Parafilm "corral". Grazing incidence conditions (incident angle = ca. 0.2°) were obtained by the angle between the horizontal X-ray beam and the natural curvature of the water surface; this curvature was low enough in comparison to the overall surface area of the water subphase, however, to prevent "slippage" of the NP/polymer film out of the X-ray beam during the self-assembly process. In situ monitoring of NP/polymer film formation was performed in an enclosed box saturated with toluene vapor to slow the rate of solvent evaporation during self-assembly to better match the frame rate of the X-ray camera (10 s total with 5 s integration and 5 s read times) as well as to minimize changes in water level height due to subphase evaporation. Kapton windows in the enclosure (overall dimensions = 125 × 100 × 25 mm) provided access for incident and scattered X-rays. The vertical height of the subphase was adjusted using a motorized stage to bisect the incident beam. After initiation of data collection, a remote-controlled syringe was used to dispense a drop of NP/polymer solution (6 μL of 5 mg/mL NP and 5 to 10 mg/mL PMMA in toluene) onto the water surface.

Figure 2 presents representative 2D GISAXS data obtained during the in situ observation of Au NP/PMMA assembly (NP/polymer mass ratio = 1:1), with t = 0 s defined by the release of the toluene droplet. It is apparent that assembly of the final ordered Au NP lattice occurs through an intermediate phase at lower q_y characterized by a broad line width with q being consistent with the nearest interparticle distance of liquidlike 2D closed-packed nanoparticles (~80 Å). Like the final lattice, this phase is two-dimensional, as determined by the rodlike shape and orientation (along q_z) of the scattering feature (Bragg rod). Also, the mechanism of transformation between the two phases appears to be a discontinuous pathway. To better understand this transformation, horizontal linecuts were extracted from the full sequence of data at q_z = 0.03 ± 0.002 (sample linecuts given in Figure 3A); peak fitting was then used to extract the relative signal intensity (Figure 3B) and peak position (Figure 3C) for the two phases.

The time correlation between the relative peak areas for the two phases (Figure 3B) indicates that the second phase is produced by transformation of the initial NP film. The large overlap in time between the incipient and final NP structures can be explained by visual observation of the spreading film combined with the experimental geometry used for these GISAXS measurements. After addition of the NP/polymer/toluene drop to the water surface, the film immediately spreads

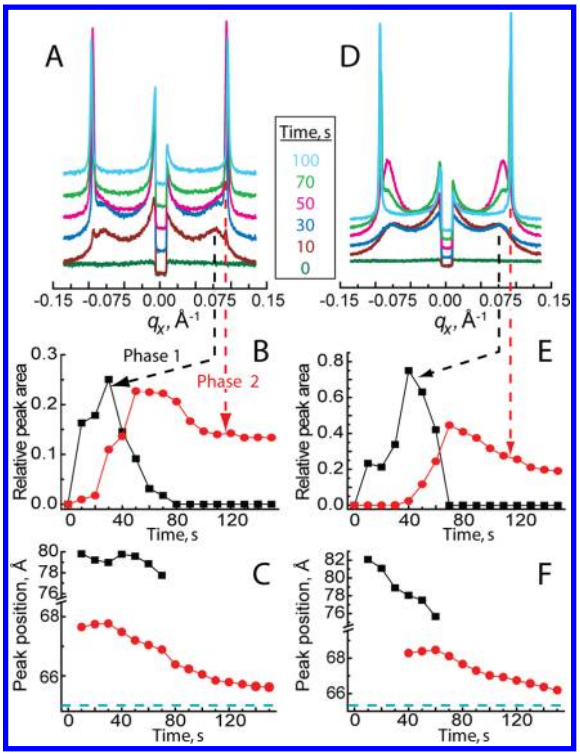

Figure 3. (A) Linecuts of 2D GISAXS images, taken at q_z = 0.03 ± 0.002, obtained during the interfacial self-assembly of a Au NP/PMMA film at a NP/polymer mass ratio of 1:1. Intensity is scaled linearly. (B) Relative peak areas of the two phases observed in A as a function of time, obtained using Gaussian fits after a spline background correction. (C) Fitted peak positions for the two phases. The dashed blue line corresponds to the final equilibrium spacing obtained at ca. 200 s. (D−F) As in panels A−C, but for a NP/polymer mass ratio of 1:2.

with a radially expanding three-phase (polymer/air/water) boundary line. The boundary then becomes pinned, and further toluene evaporation causes the film to thin radially from the boundary inward with a contracting parabolically shaped drying front (see Figure 1A). As the drying front moves radially inward, the closed packed monolayer areal fraction (whose interparticle spacing is consistent with the presence of very little toluene in the NP layer) grows inward from the film boundary at the expense of the solvated randomly packed fraction. As the X-ray beam interrogates the NP/polymer film across the entire diameter of the interfacial film in a direction approximately normal to the film boundary and drying lines, regions of film on both sides of the retracting drying line are interrogated simultaneously; thus there is substantial overlap between the two NP packing states across the beam footprint.

Peak position data (Figure 3C) indicates the compression of the initial phase, followed by an abrupt/discontinuous transformation of peak position to the final NP array with further contraction of this lattice before equilibrium is achieved. As stated previously, we assign this incipient structure to a close packed liquidlike state based upon the breadth of the scattering peak (Figure 2) combined with q being close to the expected value for interparticle spacing; this experimental interparticle distance (~78−80 Å) is less than the width of the Au NP core (55 Å) plus the length of two dodecane thiol protecting groups[22] (36 Å, for a total of 91 Å), indicating significant interdigitation between alkane chains on adjacent NPs, even at the beginning of film assembly. This degree of interdigitation

dx.doi.org/10.1021/nl304253y | Nano Lett. 2013, 13, 1041−1046

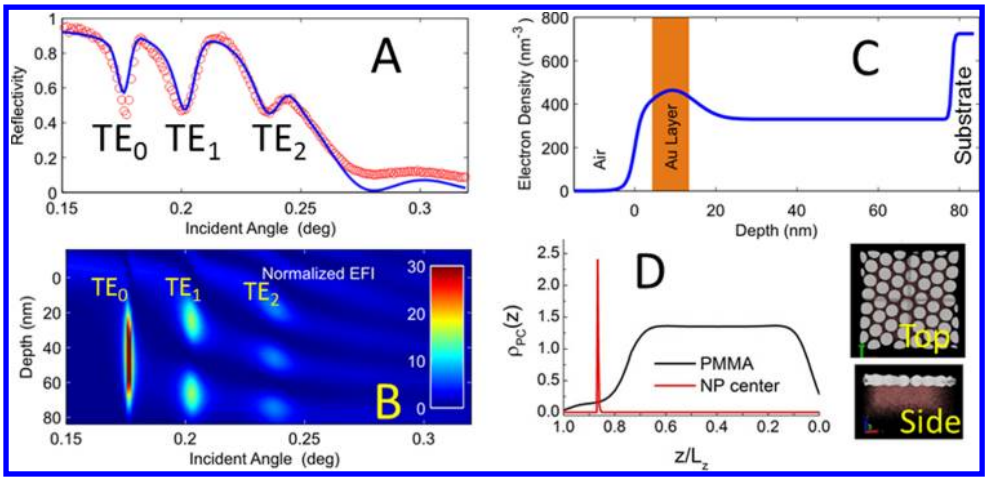

Figure 4. X-ray reflectivity (XRR) data for a Au NP/PMMA (mass ratio 1:2) monolayer showing the localization of the NP layer at the air/polymer interface during self-assembly. (A) Experimental (open circles) and simulated (solid line) XRR data with angle minima labeled with the resonant mode. (B) Electric field profile calculated for the data in panel A, showing TE_0, TE_1, and TE_2 waveguiding modes. (C) Au NP/polymer film depth profile for the simulated data of panel A, calculated using a Gaussian electron density profile for the NP layer. (D) Numerical simulation of the equilibrium distribution of NP centers in a polymer film located at a water surface. $\rho_{PC}(z)$ is proportional to the probability of finding the particle center at position z. The polymer/water and air/water interfaces are at $z/L_z = 0$ and 1.0, respectively. The inset images show the top and cross-sectional views of the nanoparticle/polymer film with white spheres representing the hard core of ligand-coated nanoparticles and red labeling polymer beads.

we observe here agrees with previous measurements of interparticle spacing between C_{12}−SH protected NPs (~30−40% of the alkane chain length).[22,23] After only a 2% compression of this disordered NP array, the peak position is reduced by a factor of about 15%, consistent with the formation of an ordered lattice where the new peak position corresponds to the (10) spacing (Figure 1B), equal to $\sqrt{3}/2$ times the interparticle distance. Even after this phase transformation, the film continues to be compressed with a further 3% reduction in peak spacing occurring before the film reaches equilibrium at ca. 200 s.

From this data, we propose a self-assembly pathway whereby an initial liquidlike NP phase, localized at the polymer−air interface via phase separation during the initial spreading and drying of the toluene droplet, is compressed at the parabolic solvent drying line to form the ordered lattice (as illustrated in Figure 1A). As a test of this mechanism, we repeated the in situ GISAXS experiment with an increased polymer concentration, keeping the amount of NPs constant, expecting that increased film mass would extend the time scale of solvent evaporation, slowing the self-assembly process relative to films with less polymer. Figure 3D−F contains this data, showing that this was indeed the case. (We note that the total film area did not increase significantly with the increase of polymer concentration within the toluene solution, indicating that the extra mass of polymer was manifested as greater film thickness and not overall spreading area.) The incipient randomly packed phase first appears at the same time (t = 10 s), consistent with deposition of NPs from the drying line of bulk toluene. Transformation into the final lattice was delayed, however, by 20−30 s, congruent with our hypothesis that formation of the ordered lattice is driven by solvent evaporation from the polymer film. Also, the temporal overlap between the two NP phases is less with increased evaporation time, likely due to the presence of a more consistent phase equilibrium across the NP/polymer film induced by slower drying kinetics. Finally, the peak position behavior as a function of time for the initial and final NP arrays is similar to the case of the film with 1:1 mass ratio between NPs and polymer with the small differences in observed spacing (~2 Å) probably attributable to experimental variation rather than changes in alkane thiol conformation or the presence of polymer between particles.

An alternate assembly mechanism that we consider is the growth of NP islands at the film/air interface by diffusion of free particles from solution, as has been observed for NP assembly at the surface of an evaporating droplet.[10] However, we reject this pathway based upon the observation that a solid film is formed upon the initial expansion of the spreading drop, preventing significant NP diffusion. Also, we do not see scattering features (e.g., rings) consistent with the presence of isolated NPs diffusing to the surface of the film through solvent or polymer. Finally, the domain size, calculated from the width of the scattering peaks along q_y, does not increase significantly before transformation to the final lattice. For the film with a NP/polymer mass ratio of 1:1, the domain size increases from ~32 to 50 nm, an increase of only two particle diameters, while for the film with mass ratio of 1:2, this only increases from ~40 to 50 nm. After the transformation to the final lattice, we calculate domain sizes in the range of 350 to 400 nm.

An important component to our self-assembly mechanism is the localization of the NPs at the air interface throughout the course of the interfacial self-assembly pathway as suggested by our observation that the array develops strictly as a monolayer, which due to the hydrophobic nature of the NPs would be expected to reside at the hydrophobic air interface. To conclusively demonstrate this idea, X-ray reflectivity (XRR) was combined with theoretical analysis treating the NP/polymer film as a resonance-enhanced X-ray waveguide within a generalized multilayer distorted-wave Born approximation as described previously.[24,25] Figure 4A contains XRR data for a Au NP/PMMA film (mass ratio = 1:1) transferred to a polished Si substrate through a "lifting" technique (placing the polymer interface that was formerly at the water surface onto the Si support),[2] along with a data fit using a Gaussian electron density profile for the Au NP layer. A prominent feature of the XRR data is the presence of three minima in the reflectivity

dx.doi.org/10.1021/nl304253y | Nano Lett. 2013, 13, 1041−1046

curve, each corresponding to a resonant enhancement of the electric field intensity (EFI) within the NP/polymer film[24,25] as plotted in Figure 4B (the EFI as a function of film depth and incident angle). Figure 4C shows the electron density through the film thickness as determined by the data fit in panel A. The NP layer is, in fact, localized at the polymer/air interface during film assembly, centered at 9.3 nm below the surface with a vertical Gaussian distribution of σ = 5.7 nm. Both of these values are greater than what would be expected for a planar Au NP array situated at the immediate surface when the radius of Au and length of the alkane thiol protecting group are taken into consideration (9.1 nm total thickness including the diameter of the Au NP core plus two times the alkane chain length); this discrepancy may be a result of layer roughness or imperfect planarity induced by sample transfer to the Si substrate. Finally, an overall film (alkanethiol-protected Au plus polymer) thickness of 78 nm corresponds closely with measurements by spectroscopic ellipsometry (~80 nm).

This observed phase separation between alkane-protected NPs and PMMA is consistent with previous literature[26] as well as numerical simulations of equilibrium particle positions within a water-immiscible polymer (e.g., PMMA) film at a water surface (Figure 4D; details of the simulations are given in Supporting Information). At equilibrium, the nanoparticles migrate to the upper surface of the polymer and form a closely packed array with formation of this asymmetrical structure being driven by a balance of enthalpic and entropic forces incurred for NPs located within the polymer (a result of polymer chain stretching) or at the polymer/water interface.

A compression-based self-assembly pathway suggests a comparison to the formation mechanism of LB films of monodisperse alkane-protected NPs. During the preparation of LB films,[8,9] depending on the attraction forces between NPs, particles are initially present (at low surface pressure) in either a low density "gas phase" or in isolated rafts of packed particles; upon mechanical compression, a sharp inflection point in the pressure−area isotherm indicates the formation of a continuous 2D lattice with further compression resulting in collapse of the 2D film into a multilayer structure. In the film assembly mechanism described here, the initial state of the NP lattice is already a continuous, albeit non-close-packed film, which undergoes gradual compression by a final stage of drying to form a close-packed monolayer. Like LB films, the transition between the initial and final phase is also discontinuous, although the final crystalline phase undergoes further in-plane shrinkage during continued drying. In our case, however, the discontinuity arises from the abrupt drying line that contracts radially inward, "metering" out a close-packed monolayer.

In summary, we have used in situ GISAXS to study the interfacial assembly of an ordered NP/polymer monolayer, which occurs (in the present geometry) by progressive evaporation-induced compression of a previously unknown randomly packed 2D NP/polymer intermediate layer localized at the liquid/vapor interface to form the final close-packed lattice. The localization of NPs at the polymer/air interface was confirmed through XRR. Using these insights into the formation of single component nanoparticle monolayers, we are now extending the interfacial assembly process to binary systems (Figure 1B), which to date have been formed on a confined liquid interface in a batch process by one-dimensional evaporation of a volatile solvent.[10,11] A critical question is whether binary and ternary NP self-assembly could be accomplished in a rapid continuous process amenable for large scale manufacturing. Our results showing rapid interfacial self-assembly in a traveling drying front suggest that this is possible, and future in situ GISAXS studies of these binary films (see Figure 5 for sample static GISAXS data)[11,12,10,11,10,11] will

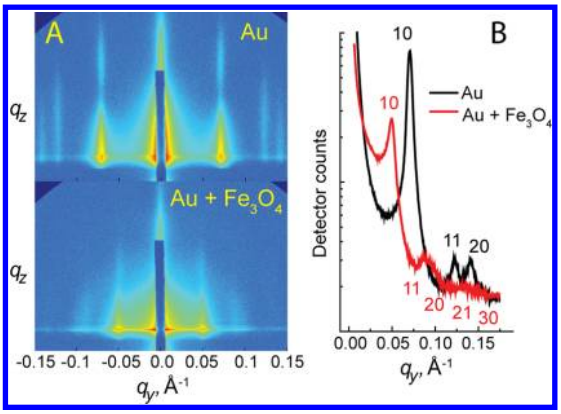

Figure 5. Data demonstrating the synthesis of binary NP lattice/polymer films using the interfacial assembly process. (A) Static GISAXS data for an Au NP (ca. 10.6 nm diameter, based on lattice spacing) /PMMA film (top) and an Au and Fe_3O_4 binary 2D NP lattice/PMMA film (bottom, with ca. 14.8 nm diameter Fe_3O_4, approximate Au: Fe_3O_4 ratio = 2:1), showing the incorporation of Au NPs into the Fe_3O_4 lattice, (B) linecuts of this data taken at q_z = 0.04 +/1 0.005 $Å^{-1}$, indexed to a hexagonal lattice, confirming the disappearance of separate Au packing,.

be critical to the optimization and scaling-up of this process. These studies will be enhanced by the recent developments of new instrumental capabilities for GISAXS (for example, high-speed X-ray cameras with subsecond frame rates[19]) that will enable more detailed investigations into the interfacial self-assembly process such as the mechanism of phase separation between NPs and polymer at the toluene/air drying line and how to maximize the rate of interfacial self-assembly.

■ ASSOCIATED CONTENT

Ⓢ Supporting Information

Additonal information, figures, and video. This material is available free of charge via the Internet at http://pubs.acs.org.

■ AUTHOR INFORMATION

Corresponding Author

*E-mail: (D.R.D.) ddunphy@unm.edu; (C.J.B.) cjbrink@sandia.gov.

Present Address

⊥Institute for Molecular Engineering, University of Chicago, Chicago IL 60637, United States.

Notes

The authors declare no competing financial interest.

■ ACKNOWLEDGMENTS

This work was supported by DOE Basic Energy Sciences grant DE-FG02-02-ER15368, the DOE Office of Basic Energy Sciences Molecular Nanocomposite Program and NSET Program DEFG03-02ER 15638, the National Institute for NanoEngineering (NINE) program at Sandia National Laboratories, and by the Laboratory Directed Research and Development program at Sandia National Laboratories. Sandia is a multiprogram laboratory operated by Sandia Corporation, a Lockheed Martin Company, for the United States Department

of Energy's National Nuclear Security Administration under Contract DE-AC04-94AL85000. Use of the Advanced Photon Source was supported by the DOE Office of Basic Energy Sciences under Contract number DE-AC02-06CH11357. TEM experiments were performed in the TEM imaging center of the Earth and Planetary Science Department at the University of New Mexico. We thank Chris Murray and group for providing the Au and Fe_3O_4 NPs used in Figure 5.

REFERENCES

(1) Ashley, C. E.; Dunphy, D. R.; Jiang, Z.; Carnes, E. C.; Yuan, Z.; Petsev, D. N.; Atanassov, P. B.; Velev, O. D.; Sprung, M.; Wang, J.; Peabody, D. S.; Brinker, C. J. *Small* **2011**, *7* (8), 1043−1050.
(2) Xiong, S.; Miao, X.; Spencer, J.; Khripin, C.; Luk, T. S.; Brinker, C. J. *Small* **2010**, *6* (19), 2126−2129.
(3) Luk, T. S.; Xiong, S.; Chow, W. W.; Miao, X.; Subramania, G.; Resnick, P. J.; Fischer, A. J.; Brinker, C. J. *J. Opt. Soc. Am. B* **2011**, *28* (6), 1365−1373.
(4) Coe, S.; Woo, W. K.; Bawendi, M.; Bulovic, V. *Nature* **2002**, *420* (6917), 800−803.
(5) Robel, I.; Subramanian, V.; Kuno, M.; Kamat, P. V. *J. Am. Chem. Soc.* **2006**, *128* (7), 2385−2393.
(6) Grunes, J.; Zhu, J.; Anderson, E. A.; Somorjai, G. A. *J. Phys. Chem. B* **2002**, *106* (44), 11463−11468.
(7) Liu, J.; Lee, T.; Janes, D. B.; Walsh, B. L.; Melloch, M. R.; Woodall, J. M.; Reifenberger, R.; Andres, R. P. *Appl. Phys. Lett.* **2000**, *77* (3), 373−375.
(8) Guo, Q. J.; Teng, X. W.; Rahman, S.; Yang, H. *J. Am. Chem. Soc.* **2003**, *125* (3), 630−631.
(9) Heath, J. R.; Knobler, C. M.; Leff, D. V. *J. Phys. Chem. B* **1997**, *101* (2), 189−197.
(10) Bigioni, T. P.; Lin, X. M.; Nguyen, T. T.; Corwin, E. I.; Witten, T. A.; Jaeger, H. M. *Nat. Mater.* **2006**, *5* (4), 265−270.
(11) Dong, A. G.; Chen, J.; Vora, P. M.; Kikkawa, J. M.; Murray, C. B. *Nature* **2010**, *466* (7305), 474−477.
(12) Dong, A. G.; Ye, X. C.; Chen, J.; Murray, C. B. *Nano Lett.* **2011**, *11* (4), 1804−1809.
(13) Lin, X. M.; Jaeger, H. M.; Sorensen, C. M.; Klabunde, K. J. *J. Phys. Chem. B* **2001**, *105* (17), 3353−3357.
(14) Pang, J. B.; Xiong, S. S.; Jaeckel, F.; Sun, Z. C.; Dunphy, D.; Brinker, C. J. *J. Am. Chem. Soc.* **2008**, *130* (11), 3284−3286.
(15) Xiong, S.; Molecke, R.; Bosch, M.; Schunk, P. R.; Brinker, C. J. *J. Am. Chem. Soc.* **2011**, *133* (30), 11410−11413.
(16) Doshi, D. A.; Gibaud, A.; Goletto, V.; Lu, M. C.; Gerung, H.; Ocko, B.; Han, S. M.; Brinker, C. J. *J. Am. Chem. Soc.* **2003**, *125* (38), 11646−11655.
(17) Doshi, D. A.; Gibaud, A.; Liu, N. G.; Sturmayr, D.; Malanoski, A. P.; Dunphy, D. R.; Chen, H. J.; Narayanan, S.; MacPhee, A.; Wang, J.; Reed, S. T.; Hurd, A. J.; van Swol, F.; Brinker, C. J. *J. Phys. Chem. B* **2003**, *107* (31), 7683−7688.
(18) Dunphy, D.; Fan, H. Y.; Li, X. F.; Wang, J.; Brinker, C. J. *Langmuir* **2008**, *24* (19), 10575−10578.
(19) Jiang, Z.; Li, X.; Strzalka, J.; Sprung, M.; Sun, T.; Sandy, A. R.; Narayanan, S.; Lee, D. R.; Wang, J. *J.Synchrotron Radiat.* **2012**, *19*, 627−636.
(20) Narayanan, S.; Wang, J.; Lin, X. M. *Phys. Rev. Lett.* **2004**, *93*, 13.
(21) Prasad, B. L. V.; Stoeva, S. I.; Sorensen, C. M.; Klabunde, K. J. *Langmuir* **2002**, *18* (20), 7515−7520.
(22) Giersig, M.; Mulvaney, P. *Langmuir* **1993**, *9* (12), 3408−3413.
(23) Park, Y.-K.; Park, S. *Chem. Mater.* **2008**, *20* (6), 2388−2393.
(24) Jiang, Z.; Lee, D. R.; Narayanan, S.; Wang, J.; Sinha, S. K. *Phys. Rev. B* **2011**, *84*, 7.
(25) Narayanan, S.; Lee, D. R.; Guico, R. S.; Sinha, S. K.; Wang, J. *Phys. Rev. Lett.* **2005**, *94*, 14.
(26) Balazs, A. C.; Emrick, T.; Russell, T. P. *Science* **2006**, *314* (5802), 1107−1110.